

# Modeling of Lithium Granule Injection in NSTX using M3D-C1

A. Fil<sup>1</sup>, E. Kolemen<sup>1</sup>, N. Ferraro<sup>2</sup>, S. Jardin<sup>2</sup>, P.B. Parks<sup>3</sup>, R. Lunsford<sup>2</sup>, R. Maingi<sup>2</sup>

<sup>1</sup>Princeton University, NJ 08540, USA

<sup>2</sup>Princeton Plasma Physics Laboratory, Princeton, NJ 08543, USA

<sup>3</sup>General Atomics, PO Box 85608, San Diego, CA 92186, USA

*E-mail contact of main author: afil@pppl.gov*

**Abstract.** In this paper, we present simulations of pedestal control by Lithium Granule Injection (LGI) in NSTX. A model for small granule ablation has been implemented in the M3D-C1 code [1], allowing the simulation of realistic Lithium granule injections. 2D and 3D simulations of Li injections in NSTX H-mode plasmas are performed and the effect of granule size, injection angle and velocity on the pedestal gradient increase is studied. The amplitude of the local pressure perturbation caused by the granules is found to be highly dependent on the solid granule size. Adjusting the granule injection velocity allows one to inject more particles at the pedestal top. 3D simulations show the destabilization of high order MHD modes whose amplitude is directly linked to the localized pressure perturbation, which is found to depend on the toroidal localization of the granule density source.

## 1. Introduction

ITER will have to keep the pedestal free of Edge-Localized-Modes (ELMs) to prevent large heat fluxes potentially damaging for the device. At the same time, ITER must maintain very high plasma performance to reach its goals. To achieve this, real-time pedestal control will need to be used in ITER as well as in future fusion reactors. NSTX and other devices have already developed and tested many different control schemes in order to adjust and regulate the pedestal pressure and density. The aim is to change the pedestal parameters to mitigate ELMs. For example, gas puffing [2] injects fuel or impurities at the plasma edge to control the plasma pedestal density, 3D magnetic perturbations [3] create an edge stochastic layer increasing the transport (which lowers the pedestal pressure gradient), Lithium Granule Injections (LGI) [4] induce pressure perturbations triggering ELMs and can thus change the ELM frequency and their impact on the Plasma Facing Components (PFCs). NSTX-U is currently planning additional tests of these methods, in particular for LGI. The next step would be to combine all these methods into an adaptive and automatic pedestal control algorithm for tokamaks. Such a capability could allow one to explore new innovative scenarios such as the Super H-Mode [5] or lithium induced ELM-free regimes [6]. To build such a control algorithm, simplified models must be derived based on our understanding of the physics and on how the different control actuators affect the pedestal. This is especially important in order to evaluate applicability to future reactors, e.g. ITER.

In this paper, we focus on the LGI technique only and present numerical simulations of granule induced perturbations to the plasma with the code M3D-C1. M3D-C1 [1] is a state-of-the-art 3D full-MHD code with realistic geometry and is being developed to study the non-linear plasma response when several actuators are triggered (gas puffing, 3D magnetic perturbations and LGI). Few high frequency Li granule injections have been performed experimentally in DIII-D [7] and EAST and a LGI system has recently been installed on NSTX-U. As it is using non-fuel, non-recycling materials, LGI allows a decoupling of ELM control from plasma fueling. DIII-D experiments have demonstrated a robust ELM-pacing and a triggering efficiency higher than 80% for 0.9 mm lithium granules, but some concern exists because of the variability of

triggered-ELM sizes. In particular, in high density, low-torque ITER baseline scenarios, an increase of the ELM frequency by LGI-pacing did not directly translate in ELM size mitigation [8]. Modeling with M3D-C<sup>1</sup> investigates these phenomena by simulating the non-linear, 3 dimensional dynamic evolution of a realistic tokamak equilibrium subject to a triggered ELM. For this study, ablation models for Lithium granules have been implemented in M3D-C<sup>1</sup>. Studies of LGI with M3D-C<sup>1</sup>, whose first steps are detailed in this paper, improve our physical understanding of this method and will allow us to build reduced models for control applications. First, we present the implementation of granule ablation models in M3D-C<sup>1</sup>. We will then present the results of 2D NSTX LGI simulations investigating the pressure perturbation triggered by different granule sizes, injection angle and velocity. Finally, we will present 3D simulations investigating the MHD activity triggered by LGI.

## 2. Implementing ablation models for lithium granules in M3D-C<sup>1</sup>

Two models have been implemented in M3D-C<sup>1</sup> to calculate the ablation rate of the Lithium granule. The first one [9] [10] is a Neutral Gas Shielding Model calibrated on DIII-D experimental measurements of the Lithium granule ablation rates. The second one [11] is valid for small size granules (sub-mm) where the contribution of plasma ions to the granule ablation is not negligible. In this second model, the ablation flow is treated as an expanding monoatomic gas with spherical symmetry, and a realistic Maxwellian distribution function for incident fast electrons is used. It also accounts for slowing down and pitch-angle scattering collisions of these fast electrons with cloud atoms. The granule is then modeled as a varying density source that is a Gaussian multiplied by the normalized ablation rate  $A_r$ . The realistic granule radius  $r_p$  is multiplied by an arbitrary parameter to give the width of the density source. Indeed, experimentally an ablation cloud is observed around the granule and this parameter is used to mimic the experiment. Note that this is the only "free" parameter of the granule model and that experimentally its value is difficult to measure accurately (between 5-100 times the solid granule radius). Its impact on the simulations will be discussed further when presenting the results.

At each time-step, the granule ablation rate is calculated as  $A_r = C(n_e, T_e, r_p) \times X_m$ , where  $r_p$  is the granule radius and  $(n_e, T_e)$  are the electron density and temperature of the background plasma at the granule position.  $A_r$  is given in g/s, as well as  $X_m$ .  $C(n_e, T_e, r_p)$ , the non-dimensional ablation coefficient, depends on the species parameter and is determined by solving the gas dynamic equations for the ablation flow for each set of  $(n_e, T_e, r_p)$ . A function fitting these results is used in M3D-C<sup>1</sup>. The granule radius  $r_p$  and thus the source width decreases as the granule is ablated by the plasma, as  $\delta r_p / \delta t = - C(n_e, T_e, r_p) \times X_p$ .  $X_m$  and  $X_p$  embody the dominant similarity law for the strongly shielded cryogenic pellets and depends on the granule radius, the plasma density and temperature, the atomic mass of the granule and functions describing the interaction between incident plasma electrons and the granule ablation cloud. For example,  $X_m$  is calculated as  $X_m = k(\gamma - 1)^{1/3} f_L^{1/3} W^{2/3} r_p^{4/3} n_e^{1/3} T_e^{11/6} B(Z, T_e)^{2/3}$ , where  $k = 8.1468e-9$ ,  $Z$  is the atomic number of the atomic species comprising the granule,  $W$  is the atomic mass of this species (in amu),  $\gamma$  is the effective ratio of specific heats of the ablation cloud,  $f_L$  is the flux limiter,  $r_p$  is the instantaneous granule radius (in cm),  $n_e$  is the host plasma electron density (in cm<sup>-3</sup>) and  $T_e$  is the host plasma electron temperature (in eV). More details on the model can be found in [10][11].

## 3. LGI simulations with M3D-C<sup>1</sup>

The simulations presented in the following start from NSTX experimental profiles (electron

density and temperature). The target plasma is an ELMy H-mode (plasma discharge 129015) [6] with reliable temperature measurements during the inter-ELM period (See Figure 1 showing the input profiles). The main parameters of this discharge are  $B_T = 0.44$  T,  $I_p = 0.785$  MA,  $a = 0.627$  m. The simulation is initiated within an inter-ELM time interval, at 0.4 s from the beginning of the discharge. The separatrix is at  $R = 1.48$  m and the top of the pressure pedestal is initially at  $R = 1.46$  m (see Figure 2).

In M3D-C1, we use a single-fluid resistive MHD model that assumes fast equilibration with anisotropic thermal conduction. Braginskii temperature-dependent values are used for resistivity, isotropic viscosity and conductivity.

2D simulations are performed with granule injections of different granule radius, initial speed, injection angle and size of the ablation cloud, as summarized in table 1:

$r_p$ (in mm)	Inj. Velocity (in m/s)	Source width (in cm)	Inj. angle (in degree)
0.2 – 1	50 – 200	1 - 5	-75 to +75

Table 1: Range of granule input parameters used in the simulation

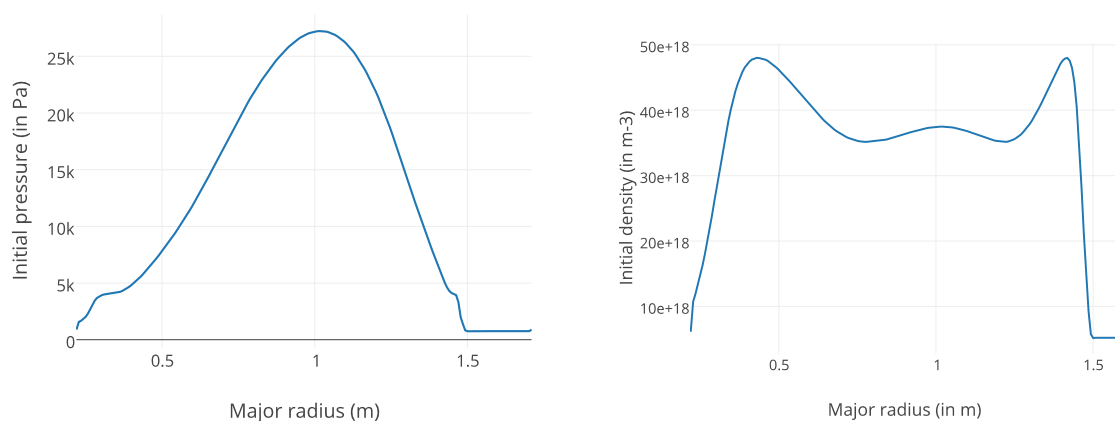
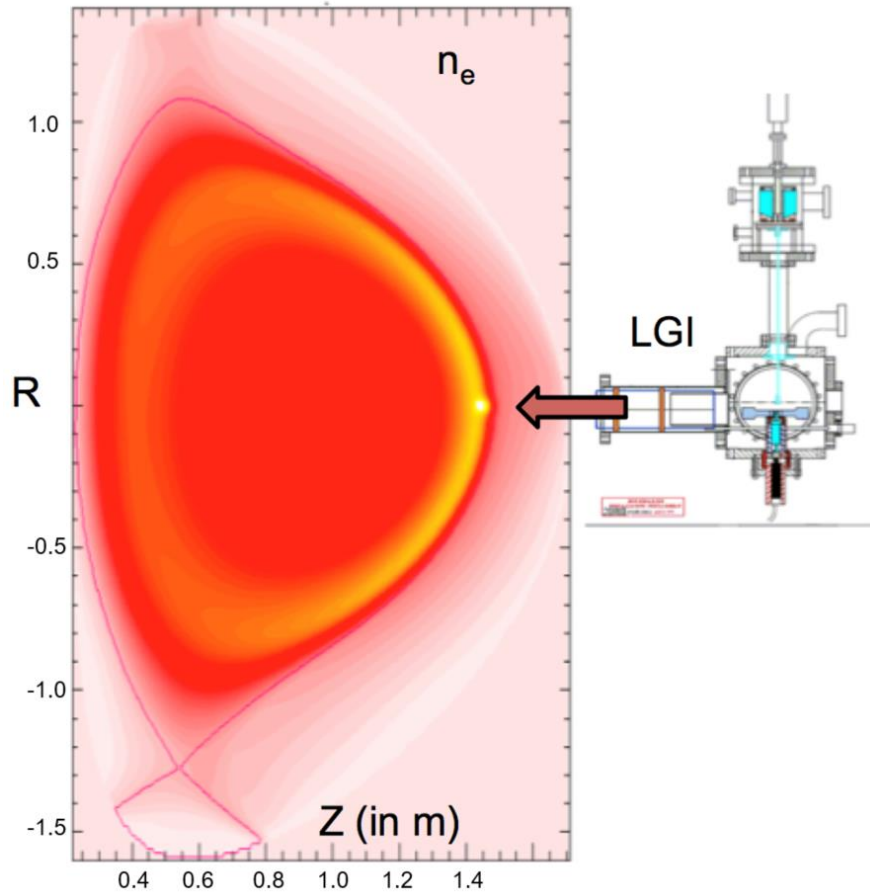


FIG. 1. Initial NSTX pressure and density profiles (before firing a Lithium Granule). These are experimental profiles within an inter-ELM time interval.

Typical meshes sizes used in the simulations are 1 - 5 mm and the time step is between  $10^{-8}$  and  $10^{-7}$  seconds. The mesh is also refined around the separatrix and where the granule is injected. In these simulations, the granule starts propagating inward at  $R = 1.5$  m with a constant velocity. In the 2D simulations, we assume a fast-toroidal equilibration of the density perturbation created by the granule injection. This way, the simulations can be run for more than 10 ms and we can study the value of the ablation rate for the full ablation process. This assumption will be relaxed in the 3D simulations where the toroidal dynamic of the density perturbation will be simulated and its impact on the MHD will be studied. As soon as the granule reaches the pedestal, a large and localized plasma electron density increase is generated (see Figure 2). Note here that there is no equation solved for the impurity density and that the source is a source of electrons. Electron conduction along the field lines reheats the localized region of high density, leading to a large increase of the plasma pressure. Figure 3 shows successive pressure profiles after the injection of a 0.8 mm granule and the maximum pressure perturbation is reached when the ablation rate of the granule is maximal. An increase of pressure also occurs in the Scrape-Of-Layer (SOL), which is associated to the boundary conditions used in the open field lines region (constant density and pressure on the boundary).

### 3.1. Impact of the granule size

The granules are totally ablated in 0.2 to 3 milliseconds, depending on their sizes and injection velocities. Those values are consistent with experiments [7]. Comparing to previous L-mode simulations [12], the penetration depth and the ablation time is up to one order of magnitude shorter due to the higher electron density and temperature in this H-mode case.



*FIG. 2. Electron density contours in the poloidal plane. The density increase is due to the injection of a 0.8 mm granule in NSTX. Separatrix is also drawn in red. The sketch of the LGI system shows that the injection is done at midplane with a variable injection velocity.*

Pressure evolution during the injection of a 0.8mm Lithium granule in NSTX

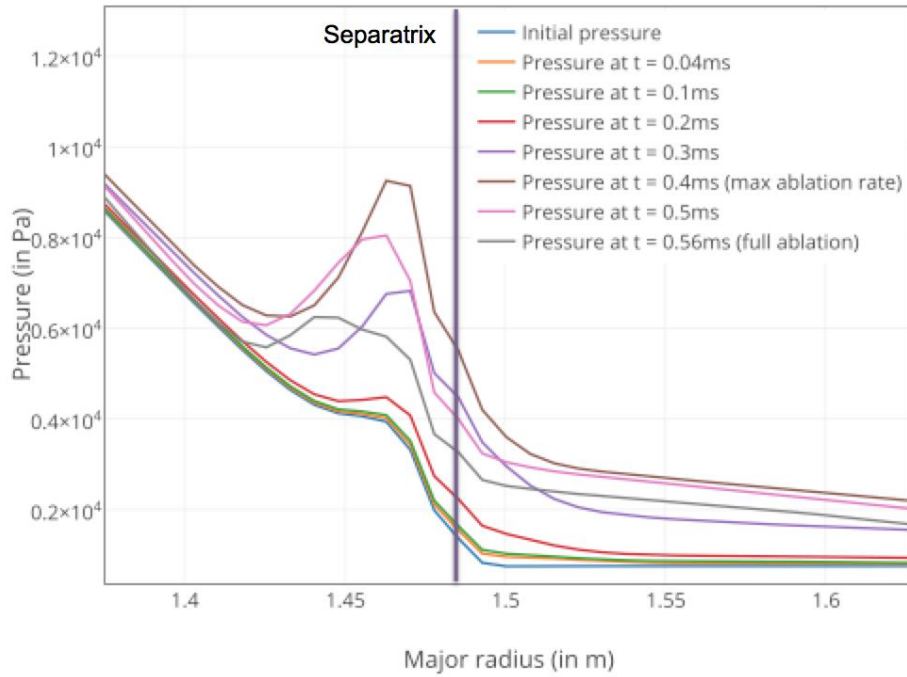


FIG. 3. Successive pressure profiles in the poloidal plan where the granule is injected. A large increase of the pedestal pressure is observed.

Figure 4 shows the positions in the plasma where the granules reach their maximum ablation rate and where the granules are totally ablated (penetration depth). The larger granules achieve a significantly larger penetration depth, up to 5.4 cm for 1 mm granules at 100 m/s, i.e. 3.4 cm inside the pedestal top.

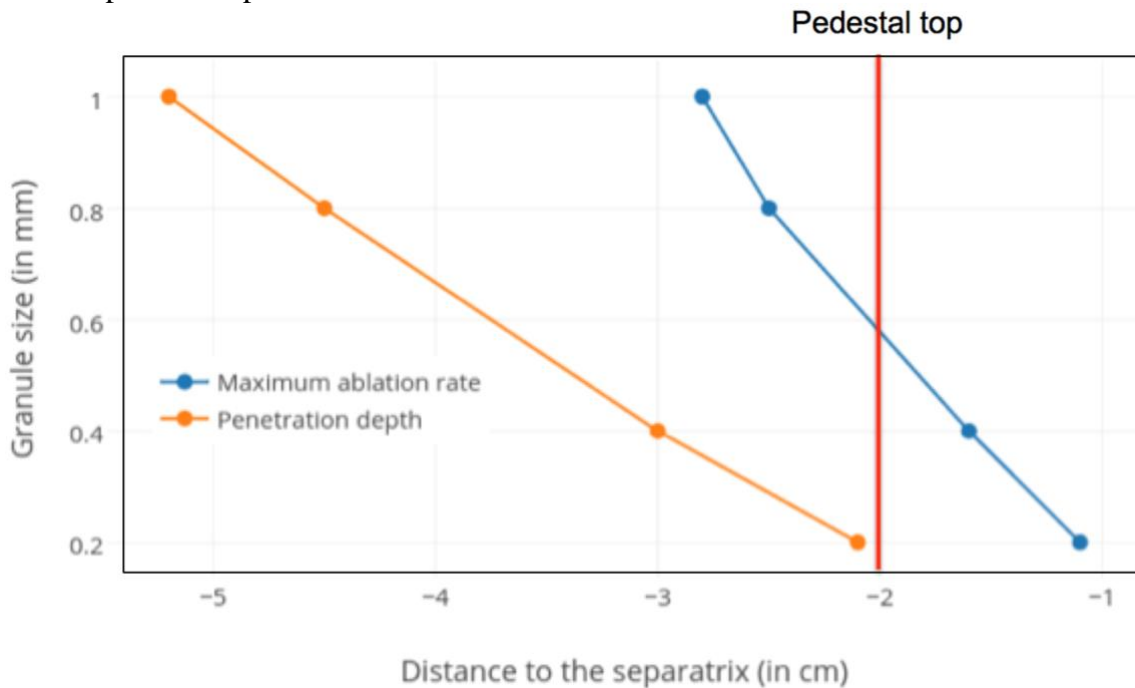


FIG. 4. Positions where the granules are at maximum ablation and where the granules are completely ablated, for different granule initial sizes and a velocity of 100 m/s. Distance is given in cm inside the separatrix (at  $r = 0$  cm) and the position of the pedestal top (at  $r = -2$  cm) is given.

The large granules inject a higher number of particles at the pedestal top but they also inject a non-negligible number of particles inside the separatrix. It is preferable for ELM triggering as it leads to a higher localized pressure perturbation. However, a granule which is too large can lead to a degradation of confinement. A compromise has to be found between the efficiency of ELM pacing and the plasma fueling resulting from large granules.

### 3.2. Impact of the granule injection velocity

For a specific granule, changing the injection velocity also changes the penetration depth and the deposition of particles, as can be seen on Figure 5. For this specific discharge, granules launched with a velocity of 50 m/s deposit more particles in the pedestal region and lead to a smaller increase of density (and temperature decrease) within the hot plasma region bounded by the pedestal top, compared to granules at 100 m/s and 200 m/s. Moreover, the particle deposition is spread and its maximum is a few centimeters inside for the fast granules compared to slower ones. It results in a lower pressure perturbation for the fast granules compared to the pressure perturbation induced by slower ones, as can be seen on Figure 6. This result shows the importance of the injection velocity and one should choose this velocity to maximize the deposition in the pedestal region. Note that in the current model the granule velocity is assumed constant and that effects that may decelerate the granule are not included (for example the impact the non-uniformity of the magnetic field on the granule ablation cloud). Such effects will be included and tested in future work.

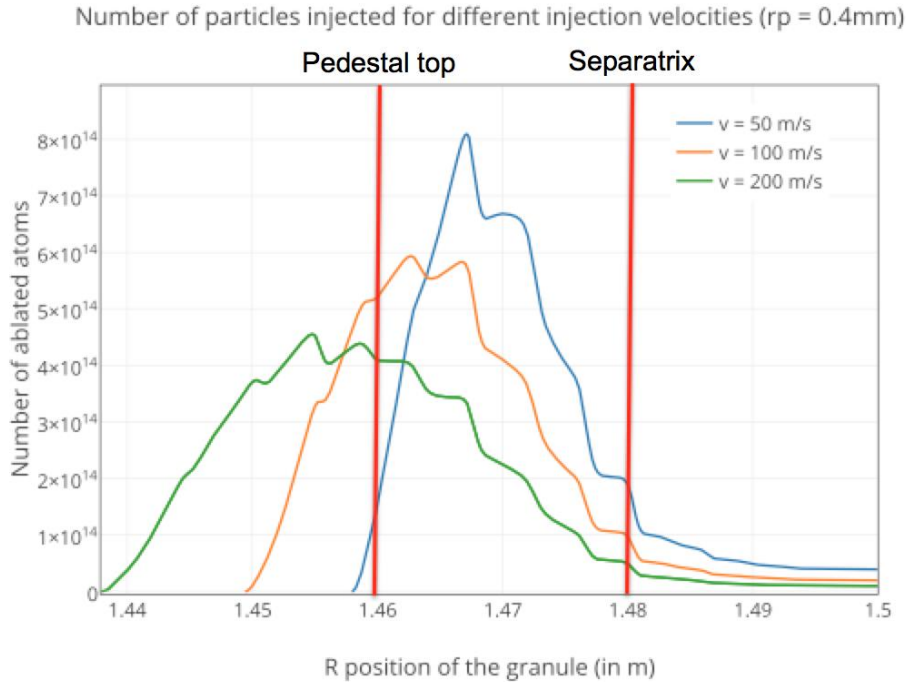


FIG. 5. Number of ablated atoms injected when the granule is penetrating into the plasma. 0.4 mm granules with different velocities are injected. The top of the pressure pedestal is at  $R = 1.46$  m for this NSTX discharge.

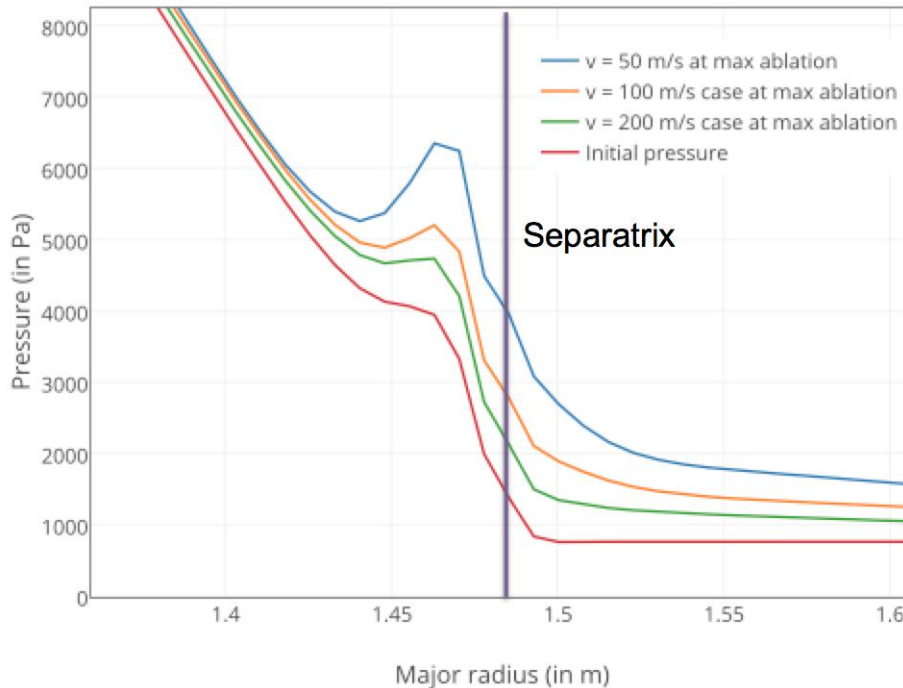


FIG. 6. Pressure profiles for different injection velocities (at maximum ablation).

Different angles of injection have also been tested in the simulations, all using a 1 mm granule. The results are that there seems to be no differences between upward and downward injections and that injecting with an angle  $\alpha$  with a velocity  $V_{inj}$  is also very similar to injecting with no angle at a velocity of  $\cos(\alpha) V_{inj}$ . However, the simulations did not consider the plasma rotation that may impact this result.

### 3.3 Impact of the ablation cloud toroidal size in 3D simulations

Finally, the impact of the size of the ablation cloud has been tested in 3D simulations. Three simulations have been done, injecting granules of the same size (i.e. same number of particles and ablation rate) but with a wider source, i.e. larger ablation cloud. The range of values is constrained by the memory limitations of the clusters that prevent us from using even finer meshes. The lower radius currently achievable for the ablation cloud is 1 cm. The radial width of the source can be varied between 1 and 5 cm and has a small impact (few %) on the maximum induced pressure perturbation. However, the toroidal width of the source has been varied in 3D simulations and has a significant impact. These simulations start from the same NSTX equilibrium and the same number of particles injected. They typically include 16 to 32 toroidal planes. The source is varied from a quasi-axisymmetric source to one with a toroidal extension of 72 degrees. The toroidal extension of the source is characterized by the parameter  $dpsi$ , which is the half width of the Gaussian in the toroidal direction.

The localized density and pressure increase is found to be much larger as the toroidal width of the source decreases. This 3D localized pressure structure is responsible for the destabilization of MHD modes, potentially leading to an ELM. In comparison, simulations done without the LGI source show no significant increase of magnetic energies in this time frame.

With the LGI source, high-order pressure-driven modes are quickly destabilized right after the Li injection. Simulations include all toroidal harmonics up to  $n = 8$  but only modes  $n=0-4$  are shown on Figure 7 ( $n=5-8$  magnetic energies are orders of magnitude lower in these

simulations). When the source width is decreased, the pressure localized peaking is higher and the magnetic energy increases faster and higher. Interestingly, the dominant magnetic mode that is destabilized is not the same for different toroidal source width. It is found to be  $n=1$  for the 120-degree case ( $d\psi = 1$ ) and  $n=4$  for the 72-degree case ( $d\psi = 0.6$ ). Numerical convergence studies have been done to validate this results. In particular, these simulations have been run with a higher number of toroidal planes and show the same results. With such extreme local parameters, one can expect new variants of peeling-ballooning modes. It is however too soon to conclude as current memory limitations on Princeton clusters prevent us from modeling further this case and to reach the highly-localized sources that are presumably required to trigger ELMs. Current priority is thus to continue these simulations on the Cori or Edison clusters (NERSC) with higher poloidal and toroidal resolutions.

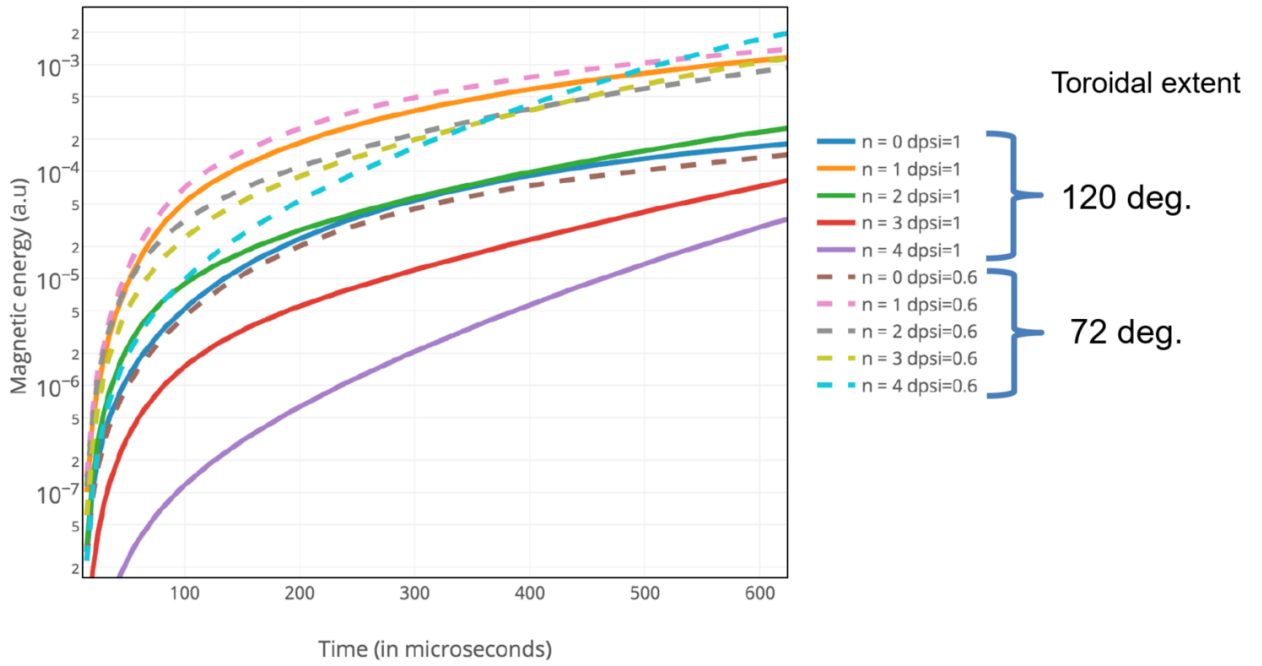


FIG. 7. Magnetic energies of harmonics  $n = 0-8$  for 3D simulations of LGI in a NSTX H-Mode plasma. Only the toroidal width of the source is varied between the two simulations.

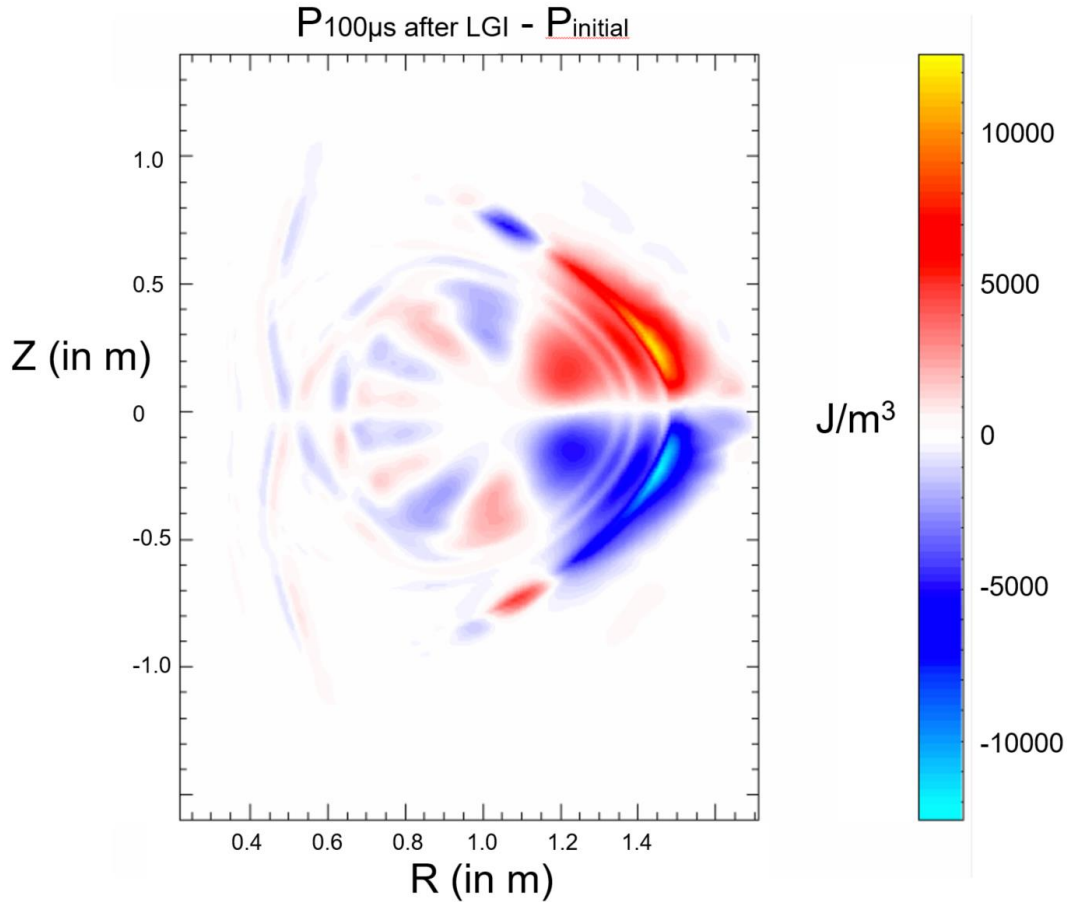


FIG. 8. Pressure perturbation between the start of the LGI and after  $100\mu\text{s}$ .

#### 4. Discussion and perspectives

These simulations show that the local pressure perturbation at the pedestal induced by LGI increases with granule size and decreases with velocity. To avoid an undesirable decrease of the temperature inside the separatrix, one can inject granules with a larger injection angle or by decreasing the injection velocity. Such granules are thus more favorable for ELM pacing. Moreover, an LGI system has been installed on NSTX-U and synthetic diagnostics (line integrated measurement of density from interferometry, heat-flux footprint in vicinity of the strike-points) are currently being implemented in M3D-C<sup>1</sup>. This will allow a comparison of the predicted density increase at the edge to the measured values.

Granules with a high injection velocity are not found to be always beneficial. A fast granule might increase the pedestal pressure gradient very quickly, but to values below the ELM-triggering threshold, when slower granules might increase the pedestal gradient above this threshold for the same number of injected particles and thus be more efficient for ELM pacing. 3D simulations are on going to specify quantitatively this threshold and the impact of granule parameters on ELM properties (ELM mode number, heat flux on the divertor plates). These simulations aim at finding an effective compromise between fast ELM-pacing and high confinement. 3D simulations already show the impact of the toroidal localization of the density source on the amplitude of the magnetic energy, in particular for high-order modes. Current effort aims at further decreasing the source toroidal localization via mesh packing techniques and adaptive meshing.

**Acknowledgments.** This manuscript is based upon work supported by the U.S. Department of Energy, Office of Science, Office of Fusion Energy Sciences, and has been authored by Princeton University under Contract Number DE-AC02-09CH11466 with the U.S. Department of Energy. The digital data for this paper can be found in <http://arks.princeton.edu/ark:/88435/dsp018p58pg29j>.

[1] S.C. JARDIN, et al., Computational Science & Discovery, 5 (2012) 014002

[2] R. NAZIKIAN, et al., Proceedings of IAEA 2014, EX1-1

[3] R.J. HAWRYLUK, et al., Nucl. Fusion 55 (2015) 053001

[4] D. K. MANSFIELD, et al., Nucl. Fusion 53 (2013) 113023

[5] W. M. SOLOMON, et al., PRL 113, 135001 (2014)

[6] R. MAINGI, et al., PRL 103, 075001 (2009)

[7] A. BORTOLON, et al., Nucl. Fusion 56 (2016) 056008

[8] A. BORTOLON, et al., to be submitted to Nuclear Fusion

[9] R. LUNSFORD, et al., Fusion Eng. Des. 112 (2016) 621-627

[10] P. B. PARKS, et al., Nuclear Fusion 34 417 (1994)

[11] P. B. PARKS, et al., to be submitted in Physics of Plasmas

[12] A. FIL, et al., Accepted for publication in Nuclear Materials and Energy